CHEMISTRY OF MATERIALS
Article

Chem. Mater. **2010,** *22,* 3197–3205 3197
DOI:10.1021/cm100294d

Nanoporous Structure and Medium-Range Order in Synthetic Amorphous Calcium Carbonate

Andrew L. Goodwin,[†,⊥] F. Marc Michel,[‡,¶] Brian L. Phillips,[‡] David A. Keen,[§,∥] Martin T. Dove,[†] and Richard J. Reeder*[,‡]

[†]*Department of Earth Sciences, University of Cambridge, Downing Street, Cambridge CB2 3EQ, U.K.,* [‡]*Department of Geosciences and Center for Environmental Molecular Science, Stony Brook University, Stony Brook, New York 11794-2100,* [§]*Rutherford Appleton Laboratory, ISIS Facility, Harwell Science and Innovation Campus, Didcot, Oxfordshire OX11 0QX, U.K., and* [∥]*Clarendon Laboratory, Department of Physics, Oxford University, Parks Road, Oxford OX1 3PU, U.K.* [⊥]*Current address: Inorganic Chemistry Laboratory, Department of Chemistry, University of Oxford South Parks Road, Oxford OX1 3QR, U.K.* [¶]*Current address: Department of Geological and Environmental Sciences, Stanford University, Stanford, CA 94305-2115.*

Received January 29, 2010. Revised Manuscript Received March 17, 2010

We adopt a reverse Monte Carlo refinement approach, using experimental X-ray total scattering data, to develop a structure model for synthetic, hydrated amorphous calcium carbonate (ACC). The ACC is revealed to consist of a porous calcium-rich framework that supports interconnected channels containing water and carbonate molecules. The existence of a previously unrecognized nanometer-scale channel network suggests mechanisms of how additives can be accommodated within the structure and provide temporary stabilization, as well as influence the crystallization process. Moreover, while lacking long-range order, the calcium-rich framework in the ACC contains similar Ca packing density to that present in calcite, aragonite, and vaterite, yielding clues of how the amorphous material converts into the different crystalline forms. Our results provide a new starting point for advancing our understanding of biomineralization as well as the development of biomimetic approaches to next-generation materials synthesis.

1. Introduction

The hard skeletal structures of many marine invertebrate organisms are initially formed from a metastable amorphous form of calcium carbonate (ACC) that eventually crystallizes to calcite or aragonite.[1,2] The absence of long-range structural order in ACC allows fabrication of intricate shapes not possible for crystalline analogues, which favor growth in specific crystallographic directions. This important biomineralization pathway has long attracted materials scientists interested in adapting this strategy for the design and fabrication of bioinspired materials with particular shapes and functions.[3,4] However, the fundamental obstacle faced by structural biologists and materials scientists alike has been the lack of a structural model of these amorphous phases. The need for such models is highlighted by fundamental questions within both communities of how crystallization is sufficiently delayed to allow material assembly over time scales required for biomineralization or experimental synthesis and then directed to form a particular crystalline polymorph. Studies have identified the importance of additives, such as magnesium, phosphate, and organic macromolecules,[5−7] but an understanding of their functional roles depends on developing suitable structural models for ACC. A structural picture is also key to understanding the interactions between ACC and structural templates thought to be involved in directed assembly during biomineralization and widely used in fabrication of thin films.[4,8−10]

Until recently, our knowledge of the structural features of ACC had largely been limited to the first-shell Ca coordination environment, obtained using Ca K-edge X-ray absorption fine structure (EXAFS) spectroscopy.[11−16]

*Corresponding author. E-mail: rjreeder@stonybrook.edu.

(1) Addadi, L.; Raz, S.; Weiner, S. *Adv. Mater.* **2003**, *15*, 959–970.
(2) Weiner, S.; Sagi, I.; Addadi, L. *Science* **2005**, *309*, 1027–1028.
(3) Dujardin, E.; Mann, S. *Adv. Mater.* **2002**, *14*, 775–788.
(4) Aizenberg, J.; Muller, D. A.; Grazul, J. L.; Hamann, D. R. *Science* **2003**, *299*, 1205–1208.
(5) Aizenberg, J.; Lambert, G.; Weiner, S.; Addadi, L. *J. Am. Chem. Soc.* **2002**, *12*, 32–39.
(6) Raz, S.; Hamilton, P. C.; Wilt, F. H.; Weiner, S.; Addadi, L. *Adv. Funct. Mater.* **2003**, *13*, 480–486.
(7) Loste, E.; Wilson, R. M.; Seshadri, R.; Meldrum, F. C. *J. Cryst. Growth* **2003**, *254*, 206–218.
(8) Mann, S.; Archibald, D. D.; Didymus, J. M.; Douglas, T.; Heywood, B. R.; Meldrum, F. C.; Reeves, N. J. *Science* **1993**, *261*, 1286–1292.
(9) Loste, E.; Meldrum, F. C. *Chem. Commun.* **2001**, 901–902.
(10) Popescu, D. C.; Smulders, M. M. J.; Pichon, B. P.; Chebotareva, N.; Kwak, S.-Y.; van Asselen, O. L. J.; Sijbesma, R. P.; DiMasi, E.; Sommerdijk, N. A. J. M. *J. Am. Chem. Soc.* **2007**, *129*, 14058–14067.
(11) Levi-Kalisman, Y.; Raz, S.; Weiner, S.; Addadi, L.; Sagi, I. *J. Chem. Soc., Dalton Trans.* **2000**, 3977–3982.
(12) Levi-Kalisman, Y.; Raz, S.; Weiner, S.; Addadi, L.; Sagi, I. *Adv. Funct. Mater.* **2002**, *12*, 43–48.
(13) Hasse, B.; Ehrenberg, H.; Marxen, J. C.; Becker, W.; Epple, M. *Chem.—Eur. J.* **2000**, *6*, 3679.
(14) Becker, A.; Bismayer, U.; Epple, M.; Fabritius, H.; Hasse, B.; Shi, J. M.; Ziegler, A. *J. Chem. Soc., Dalton Trans.* **2003**, 551.
(15) Gunther, C.; Becker, A.; Wolf, G.; Epple, M. *Z. Anorg. Allg. Chem.* **2005**, *631*, 2830.
(16) Politi, Y.; Levi-Kalisman, Y.; Raz, S.; Wilt, F.; Addadi, L.; Weiner, S.; Sagi, I. *Adv. Funct. Mater.* **2006**, *16*, 1289–1298.

Published on Web 04/21/2010

Indeed many of the tools traditionally used for structural characterization have found application mainly for distinguishing ACC from crystalline forms, including calcite, aragonite, vaterite, and the hydrated phase monohydrocalcite. Conventional X-ray diffraction reveals broad, diffuse maxima, consistent with the absence of long-range order, so that structure cannot be determined by traditional crystallographic methods. Infrared spectroscopy has shown that absorption bands present in crystalline calcium carbonates may be shifted, split, or attenuated in ACC,[5,15,17] and bands attributable to water molecules are readily observed in some ACC forms.

Using these techniques, studies of biological samples have identified different types of ACC. Addadi et al.[1] made a general distinction between ACC varieties that crystallize readily or remain (meta)stable in vivo, denoting these as "transient" and "stable" forms, respectively. So-called stable ACC, however, generally transforms to crystalline anhydrous calcium carbonate once isolated and exposed to water or high humidity. Addadi et al. also noted that transient ACC forms typically contain very little molecular water, whereas most stable forms are hydrated, commonly having a formula near $CaCO_3 \cdot H_2O$. Because transient, anhydrous ACC forms have been considered the precursors of crystalline skeletal parts, they have received much of the focus from structural biologists. A recent study of biomineralization of sea urchin spicules, however, suggests that hydrated ACC is the likely precursor of the anhydrous form,[18] raising the possibility that hydrated ACC plays a broader role than previously thought and that its transformation may occur via multiple steps.

ACC is readily synthesized from low- and ambient-temperature solutions containing dissolved calcium and carbonate salts, and indeed, this provides the basis for bioinspired applications. These ACC samples are nearly always hydrated, usually with a composition close to $CaCO_3 \cdot H_2O$. X-ray diffraction analysis (XRD), extended X-ray absorption fine structure (EXAFS), and infrared (IR) studies have shown that synthetic ACC samples share some similarities with hydrated biological ACC.[15] Yet, with the exception of EXAFS, which provides information on first-shell Ca coordination, these techniques have generally provided little detailed structural information for either synthetic or biogenic samples. The lack of a structure model for any of the forms of ACC poses a barrier to achieving a next-level understanding of the factors that control temporary stabilization, directed assembly, and crystallization behavior of ACC.

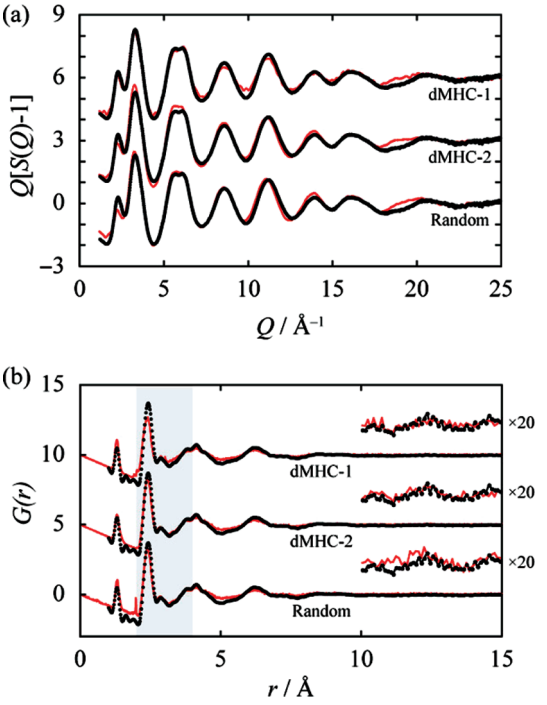

Figure 1. Comparison between modeled (red lines) and experimental (dots) X-ray total scattering data. (a) Reciprocal space $Q[S(Q) - 1]$ RMC fits for the three models described in the text. The poor agreement at 18−20 $Å^{-1}$ is due to data normalization. (b) Effective X-ray PDF function $G(r)$ formed by Fourier transform of the experimental $S(Q)$ (eq 2), compared with the reconstructed PDF functions obtained using eq 64 in ref 26 calculated from the RMC models; these functions were not fitted at all for the dMHC-1 model and were only fitted qualitatively over the range $2 \le r \le 4$ Å in the dMHC-2 and Random models (shaded region). The signature of medium range order is found in the oscillations that persist for $r > 4$ Å, shown with the corresponding RMC calculations at 20× magnification.

A significant recent advance has been the use of synchrotron X-ray total scattering methods to determine the effective atomic pair distribution function (PDF) in ACC.[19,20] The PDF is a quantitative measure of the distribution of interatomic separations, weighted by the scattering power of the various atom pairs.[21,22] It is not restricted to correlations involving a specific element, like X-ray absorption spectroscopy, and is capable of revealing atomic correlations over much greater length scales. The PDFs obtained for ACC samples synthesized using several different methods were shown to differ from those of crystalline calcium carbonate phases, both hydrated and anhydrous, but they also revealed the presence of medium-range order (MRO) up to 12−15 Å, which was previously unknown.[19] The interpretation of some features in the PDF (Figure 1b) was inferred directly.[19] For example, the two prominent peaks at ~1.3 and ~2.4 Å can be readily attributed to the C−O distance in CO_3 groups and the mean Ca−O distance, respectively. A smaller

(17) Beniash, E.; Aizenberg, J.; Addadi, L.; Weiner, S. *Proc. R. Soc. London Ser. B-Biol. Sci.* **1997**, *264*, 461–465.
(18) Politi, Y.; Metzler, R. A.; Abrecht, M.; Gilbert, B.; Wilt, F.; Sagi, I.; Addadi, L.; Weiner, S.; Gilbert, P. U. P. A. *Proc. Nat. Acad. Sci.* **2008**, *105*, 17362–17366.
(19) Michel, F. M.; MacDonald, J.; Feng, J.; Phillips, B. L.; Ehm, L.; Tarabrella, C.; Parise, J. B.; Reeder, R. J. *Chem. Mater.* **2008**, *20*, 4720–4728.
(20) Strictly speaking, Fourier transformation of the X-ray total scattering data provides the spatial correlation function of the electron density. The PDF between atom centers is not measured in the X-ray scattering experiment in the same way as in a neutron scattering experiment. To account for this, one must "sharpen" the X-ray PDF by scaling the X-ray total scattering function with a Q-dependent function representing the average scattering and then Fourier transforming this scaled scattering function. As a result, we obtain an effective PDF.
(21) Dove, M. T.; Tucker, M. G.; Keen, D. A. *Eur. J. Mineral.* **2002**, *14*, 331–348.
(22) Billinge, S. J. L.; Kanatzidis, M. G. *Chem. Commun.* **2004**, 749–760.

contribution to the peak centered at 2.4 Å can be assumed from the O−O distance of 2.2 Å in the triangular CO_3 group. However, the origin of most other features, particularly of the broader contributions at larger distances, is not at all clear. The origin of this medium-range order and its implications for the physical properties of ACC, including its stabilization and transformation pathway to crystalline forms, remain critical unanswered questions. What has been urgently needed is a method of converting the one-dimensional representation of structure reflected in the PDF into a three-dimensional model of local structure in ACC.

In this paper, we use experimental X-ray total scattering data to develop a local structure model of synthetic, hydrated ACC, where our analysis makes use of the reverse Monte Carlo (RMC) method. This approach has been applied successfully to glasses, nanocrystalline solids, and disordered crystalline solids.[23−25] The refinement procedure is based on the Metropolis Monte Carlo algorithm, in which changes in the fit to the total scattering data provide the basis for accepting or rejecting random atom movements according to the Monte Carlo algorithm. Whereas "traditional" structure refinements of crystalline materials account for long-range order through atom positions in a unit cell, RMC provides a means for evaluating the essential atom correlations, which, in the case of noncrystalline materials, provide information regarding short- and medium-range order. The correlations that evolve during the RMC fitting process are shown to be reproducible across successive independent refinements, and it is these correlations that form the basis of our analysis. The converged structure model is consistent not only with total scattering data but also with Ca K-edge X-ray absorption spectroscopy and NMR spectroscopy results. Surprisingly, our model reveals the existence of a nanoporous, charge-separated structure for hydrated ACC, suggesting both a mechanism for the stabilizing role of additives and a key feature in the transformation pathway. These new findings may have broader application to other varieties of ACC and offer new insight to strategies for design of functional materials.

2. Experimental Procedures

2.1. ACC Samples and X-ray Total Scattering. The X-ray total scattering data were collected for ACC samples at beamline sectors 1-ID and 11-ID-B at the Advanced Photon Source, Argonne National Laboratory, using synchrotron radiation (90−100 keV) out to $Q_{max} = 27$ Å^{-1}.[19] Michel et al. also describe the two methods used for synthesis of the hydrated ACC, both having approximate sample compositions of $CaCO_3 \cdot H_2O$ (also see Supporting Information, Text 1). The X-ray total scattering data from the synthetic, hydrated ACC samples are nearly identical, exhibiting broad features characteristic of noncrystalline solids (Figure 1a). These metastable ACC samples transformed to calcite within 1 week following data collection.

The pair distribution function, $G(r)$, defined as

$$G(r) = \frac{2}{\pi}\int_0^{Q_{max}} Q[S(Q) - 1]\sin(Qr)\mathrm{d}Q \quad (1)$$

was obtained by Fourier transformation of the total scattering structure factor, $S(Q)$, given by

$$S(Q) = \frac{\frac{1}{N}\frac{\mathrm{d}\sigma}{\mathrm{d}\Omega}(Q) - \sum c_i|f_i(Q)|^2}{\left|\sum c_i f_i(Q)\right|^2} + 1 \quad (2)$$

where $(1/N)(\mathrm{d}\sigma/\mathrm{d}\Omega)$ is the scattering cross-section, c_i and f_i are the atomic concentration and X-ray form-factor, respectively, for atom type i, and Q_{max} is the maximum measured value of Q. Corrections account for background, absorption, instrumental contributions, and Compton scattering. The relationships between $G(r)$ and $S(Q)$ given above and other definitions are given by Keen,[26] noting that $G(r)$ and $S(Q)$ are equivalent to $4\pi r\rho_0 G^X(r)$ and $F^X(Q)+1$ in ref 26, respectively, where ρ_0 is the sample number density.

2.2. Reverse Monte Carlo Method. RMC refinement was carried out using the program RMCProfile,[27] fitting to the Q-weighted reduced structure function, $Q[S(Q) - 1]$, from the total scattering data.[26] We used both a crystal-based model and a random model as the initial configurations, and both led to very similar final structures. Thus, we are confident that our results are independent of the initial models.

The refinement approach used a box containing a total of 1620 Ca atoms, 1620 C atoms, 4860 O_C (carbonate oxygen) atoms, and 1620 O_W (water oxygen) atoms, corresponding to a composition of $CaCO_3 \cdot H_2O$ and a density of 2.43 g cm^{-3}. Approximate dimensions are $53 \times 55 \times 45$ Å. H atoms were not included in the refinement by virtue of their insignificant contribution to the experimental X-ray scattering function. Triangular CO_3 geometries were maintained using bond-angle restraints; likewise, a set of closest-approach restraints were introduced that prevented given types of atoms from approaching one another too closely, using distances that are based on known minimum interatomic distances and sound crystal chemical intuition (see Supporting Information, Text 2). We also found that it was useful to include a soft data-based restraint on the shape of the real-space PDF between 2 and 4 Å in order to avoid a "spikiness" in the partial PDFs that commonly results from closest-approach restraints.[27] Refinements were carried out against the experimental $Q[S(Q) - 1]$ data for $1.2 \le Q \le 25.0$ Å^{-1}. Twenty independent configurations were evaluated for each refinement, and the fits and partial PDFs were taken from the average over this entire ensemble. In preparing the final structural model for visualization, illustrative H atom positions were added to the configuration using idealized O_W−H bond distances and H−O_W−H bond angles, together with the restraint that the two O_W−H bonds should be oriented as nearly as possible toward the two closest O atoms. The two starting configurations we used are described in the following sections.

As a test of our RMC approach, we also performed RMC refinements using total scattering data obtained from a calcite reference sample, collected at the same conditions as the ACC data.[19] A random starting model with composition $CaCO_3$ was used, and the same restraints were employed as for ACC fits.

(23) McGreevy, R. L. *J. Phys.: Condens. Matter* **2001**, *13*, R877–R913.
(24) Tucker, M. G.; Keen, D. A.; Dove, M. T.; Trachenko, K. *J. Phys.: Condens. Matter* **2005**, *17*, S67–75.
(25) Keen, D. A.; Goodwin, A. L.; Tucker, M. G.; Dove, M. T.; Evans, J. S. O.; Crichton, W. A.; Brunelli, M. *Phys. Rev. Lett.* **2007**, *98*, 225501.
(26) Keen, D. A. *J. Appl. Crystallogr.* **2001**, *34*, 172–177.
(27) Tucker, M. G.; Keen, D. A.; Dove, M. T.; Goodwin, A. L.; Hui, Q. *J. Phys.: Condens. Matter* **2007**, *19*, 335218.

2.2.1. Disordered Monohydrocalcite (dMHC) Starting Model. A $5 \times 6 \times 6$ supercell of the monohydrocalcite crystal structure[28] was converted to orthogonal coordinates, giving a box of dimensions $52.8 \times 54.8 \times 45.2$ Å that contained 1620 formula units $CaCO_3 \cdot H_2O$. The RMCProfile program was used to randomize the distribution of atoms in this configuration without any refinement against experimental data. However, a geometric restraint was employed to maintain triangular CO_3 units, and closest-approach restraints were used between atoms (see Supporting Information, Text 2 for further details). After randomization, none of the original coordination connectivity of the MHC structure was maintained in this process, except within CO_3 units. This disordered model, with H atoms removed, was then used as a starting configuration for RMC refinement against experimental data. We refer to this starting model as dMHC.

2.2.2. Random Starting Model. A total of 1620 Ca atoms, 1620 C atoms, 4860 O_C atoms, and 1620 O_W atoms were distributed entirely randomly throughout a configurational box of identical dimensions to that described for the dMHC model above. Each C atom was assigned three randomly allocated O_C atoms as "neighbors" (these were not necessarily located near one another), and the geometric restraints in RMC used to recover appropriate CO_3 geometries. Again, the entire configuration was randomized using the RMCProfile algorithm without refinement against experimental data and subjected only to a restraint on CO_3 geometry and closest-approach restraints. This randomized model (Random) was used as our second starting configuration for RMC refinement against experimental total scattering data.

2.3. Calculation of Ca K-Edge EXAFS Spectra. Inasmuch as Ca K-edge EXAFS spectroscopy has been used extensively to characterize the local coordination around Ca atoms in biogenic and synthetic ACC samples, including the samples used in this study,[19] we compared the EXAFS calculated for our RMC refinement model with corresponding experimental EXAFS spectra. For the present study, the Ca K-edge EXAFS signal was calculated for 100 clusters from our converged RMC configuration using the FEFF7 code,[29] with the amplitude reduction factor, S_o^2, set at 0.8. In order to assess what level of agreement might be considered reasonable, we also calculated the Ca K-edge EXAFS spectrum for calcite from our converged RMC configurations using total scattering data for the calcite reference sample. Because the local Ca coordination environment is well constrained even by the Bragg contribution to these scattering data, we anticipated that RMC should provide a very realistic description of local structure in calcite. Any difference between the calculated and observed EXAFS spectra serves as a measure of the inherent limitations of such a comparison. For example, our FEFF7 calculations do not fully account for empirical normalization or for k-dependent signal attenuation, and so, the comparison of absolute intensities should not be considered quantitative.

3. Results and Discussion

3.1. RMC Refinement. The RMC refinement method was used to evaluate the two starting configurations described in Section 2.2, both corresponding to the bulk composition ($CaCO_3 \cdot H_2O$) and density (2.43 g/cm^3) of hydrated ACC. On convergence, nearly identical fits-to-data and individual partial PDFs were obtained for the disordered monohydrocalcite starting configuration (dMHC) and for the Random starting configuration (Figure 1). It is noteworthy that an almost entirely unconstrained fit (except for restraints on the CO_3 molecular geometry) using the dMHC configuration reproduced the scattering data well (dMHC-1 in Figure 1), but gave a large proportion of unphysically short Ca−C separations < 2.5 Å. Implementation of closest-approach restraints as noted in Section 2.2 prevented given types of atoms from approaching too closely. Implementation of a soft restraint on the shape of the real-space PDF between 2 and 4 Å resulted in clear improvement in the RMC fits (dMHC-2 in Figure 1, with the real-space constrained region shaded). These restraints were also used for the Random starting configuration (Random in Figure 1), yielding a fit nearly identical to those for the dMHC starting configuration. Moreover, because the RMC fitting process is performed in reciprocal space, driven by the Q-weighted structure function, $Q[S(Q) - 1]$, this similarity in real-space (compared to the experimental total PDF) lends strong support for this approach.

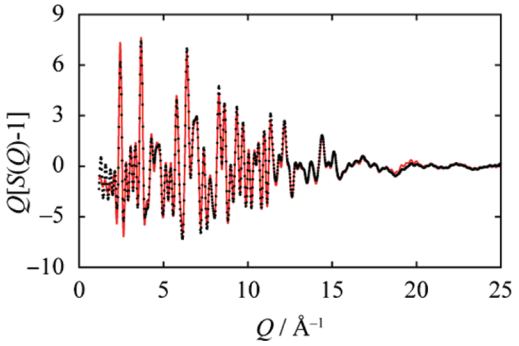

Figure 2. Comparison between modeled (red line) and experimental (dots) X-ray total scattering data for calcite reference material. Reciprocal space $Q[S(Q) - 1]$ RMC fit for the calcite data was performed in an identical manner to the ACC fits and is described in the text.

As an additional test of our approach, we performed RMC refinements using X-ray total scattering data for a calcite reference sample collected under identical conditions. Good RMC fits to data were obtained using the same restraints (Figure 2), and the resulting structure model accurately depicts the short- and long-range structure of calcite. Further validation comes from the ability of the converged RMC configurations, for both ACC and calcite, to reproduce the key features of experimental EXAFS data (as described below).

3.2. ACC Structure Model. The converged structure model derived from RMC refinement is the most disordered physical representation of ACC consistent with the experimental scattering data and the simple geometric constraints. We find only minor differences between the structure models obtained using the different starting configurations, suggesting that the overall result is largely independent of the starting configuration. Where such differences occur, we note them. We also observed that

(28) Effenberger, H. *Monatsh. Chem. Wissenschaften* **1981**, *112*, 899–909.
(29) Zabinsky, S. I.; Rehr, J. J.; Ankudinov, A.; Albers, R. C.; Eller, M. J. *Phys. Rev.* **1995**, *B52*, 2995–3009.

the key structural features of the model were present in each of the 20 individual fits.

Perhaps the most striking overall feature of the model is the evolution of two distinct, intergrown structural components: a porous calcium-rich framework and a carbonate/water component that occupies the framework channels. This key structural feature reflects an inhomogeneous distribution of Ca atoms, and hence charge, throughout the bulk material, and we discuss in greater detail below the direct experimental evidence for this Ca clustering and its likely implications for stabilization and crystallization of ACC. First, however, we describe the structure of the Ca-rich framework itself and show this to be consistent with previous local structure studies.

3.2.1. Ca-Rich Framework. In our model, we find Ca atoms bind oxygen atoms, from both carbonate ions and water molecules, with a range of coordination geometry and number (Figure 3). Particularly notable is the wide range of Ca coordination numbers, with averages of 5.3 and 5.8 (±1.5) for different starting configurations using a maximum Ca−O distance of 2.8 Å (Figure 3a). This differs from the Ca coordination environment in crystalline calcium carbonate phases, where there is a narrow distribution of coordination number in any single material and where the Ca coordination numbers themselves are higher (6 in vaterite and calcite, 8 in monohydrocalcite, and 9 in aragonite). We note that average Ca coordination numbers in our model increase by roughly one if a 3.0 Å maximum Ca−O distance is used. EXAFS investigations of ACC have reported average Ca coordination numbers from 5 to 9.[11−16] The average Ca coordination number reported by Michel et al.[19] from EXAFS fit results for the same synthetic ACC sample used in this study is 6.1 (±1.5). The value reported by Gunther et al.[15] for synthetic, hydrated ACC is 5.3 (±1.6). The large error commonly associated with EXAFS determination of coordination number makes detailed comparisons difficult. Furthermore, EXAFS studies typically report large Debye−Waller type parameters, which suggest a large distribution of first-shell Ca−O distances, and by inference coordination number, not unlike in our model results.

3.2.2. Ca-Poor Channels. By virtue of the stoichiometry and the relatively low average Ca coordination number, some carbonate ions and water molecules are left unbound by Ca, occupying instead the Ca-poor regions external to the Ca-rich framework (Figure 4). Approximately 1 nm in diameter, these carbonate/water "channels" form connected pathways. Coordinated principally via hydrogen-bonding interactions, the carbonate groups and water molecules within the channel network should be less tightly bound than those within the rigid framework, and so, the two types of each molecule should be distinguishable using appropriately sensitive experimental techniques. Indeed, NMR studies of synthetic hydrated ACC have observed two distinct populations of

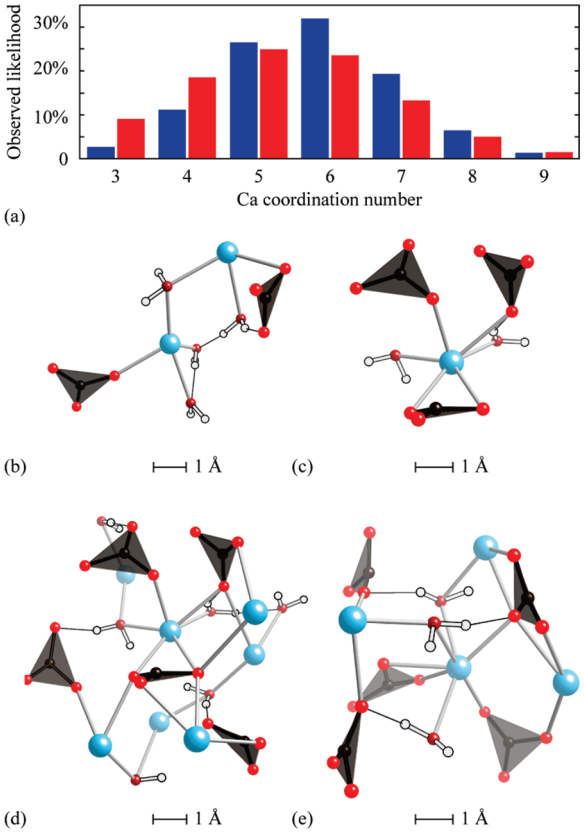

Figure 3. Ca coordination environment summary. (a) Distribution of Ca coordination numbers calculated from the dMHC-2 (blue) and Random (red) RMC refinements. (b) A representative low-coordination number Ca atom and its immediate environment. (c) A typical coordination environment of 6-coordinate Ca atoms in ACC, with the surrounding hydrogen-bonding network expanded in (d). (e) A high-coordination number Ca atom and its hydrogen-bonding environment. Calcium, carbon, oxygen, and hydrogen atoms represented as blue, black, red, and white spheres, respectively.

both water and carbonate groups, differing primarily in the mobility of associated hydrogen.[19,30] The ^{1}H NMR spectra show that about one-half of the H occurs in water molecules that exhibit restricted motion on the millisecond time scale at room temperature. The remainder of the H is primarily in rigid molecular water, except for a small fraction of hydroxyl groups. The presence of both rigid and mobile H is also evident by ^{13}C NMR, which indicates that at room temperature only about one-fourth of the carbonate groups are located near rigid molecular water. The fraction of carbonate groups near rigid H increases by a factor of about 2.3 as the temperature is lowered to −120 °C, which likely reduces the H mobility in the Ca-poor channels. There is no evidence for significant motion of the carbonate groups themselves at the millisecond time scale, which suggests that the dynamical effects are mostly related to hydrogen bond reorganization of the water/carbonate network in the Ca-poor channels. In addition, IR spectroscopy studies of ACC have identified splitting of the ν_3 C−O asymmetric stretching band in hydrated ACC,[5,31] which can be explained by multiple

(30) Feng, J. Intrinsic hydrated defects in $CaCO_3$: a solid state NMR spectroscopic study. Ph.D. Thesis, Stony Brook University, **2009**.

(31) Gayathri, S.; Lakshminarayanan, R.; Weaver, J. C.; Morse, D. E.; Kini, R. M.; Valiyaveettil, S. *Chem.—Eur. J.* **2007**, *13*, 3262–3268.

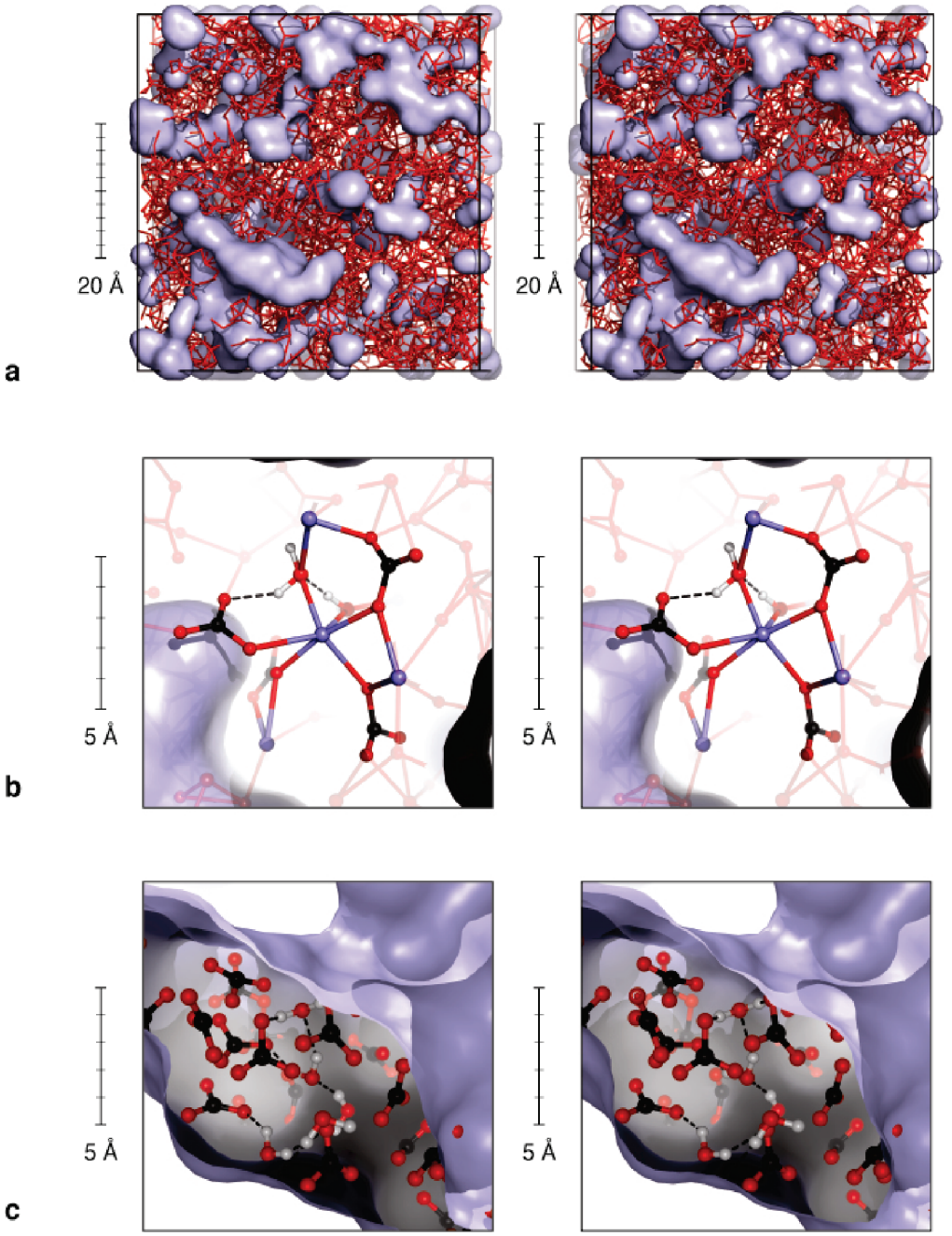

Figure 4. Stereo representations of the nanopore structure of ACC. (a) RMC model of ACC showing the Ca-rich framework in stick representation (colored red); the Ca deficient channels (regions of the structure further than 4 Å from any Ca centers) are shown in surface representation (blue). (b) Typical Ca coordination environment within the Ca-rich framework: Ca atoms in blue, O atoms in red, C atoms in black, and H atoms in white. (c) The carbonate and water molecules located within the Ca-deficient channels represent a less tightly bound structural component. Only those molecules at the surface of this channel are coordinated to nearby Ca atoms; those within the channels are bound only via hydrogen-bonding interactions.

molecular environments, and may now be rationalized in terms of the nanoscale structural inhomogeneities observed in our model. The length scale of structural inhomogeneity in our ACC is also entirely consistent with recent cryo-TEM measurements.[32]

It is useful to know if the Ca-poor channels effectively percolate the structure. Percolation in three dimensions occurs when the volume fraction of a percolating phase exceeds the critical value $\phi_c = 0.2896$.[33] In the case of ACC, the Ca-poor channels would be expected to percolate the material as long as the volume fraction of the Ca-rich framework is less than $1 - \phi_c = 0.7104$. There are different approaches to estimating this volume fraction from our RMC model, and we consider two extreme cases here.

One model for evaluating the free volume in our ACC is to consider the difference in molar volumes between hydrated ACC and calcite, 80.86 and 61.30 $Å^3$ mol^{-1},

(32) Pouget, E. M.; Bomans, P. H. H.; Goos, J. A. C. M.; Frederik, P. M.; de With, G.; Sommerdijk, N. A. J. M. *Science* **2009**, *323*, 1455–1458.

(33) Lorenz, C. D.; Ziff, R. M. *J. Chem. Phys.* **2001**, *114*, 3659–3661.

respectively, which gives $\phi = 0.2419$ and $1 - \phi = 0.7581$ for ACC (See Supporting Information, Text 3 for discussion of the ACC molar volume). We expect this value of ϕ to provide a lower bound for the true free volume, since the coordination number of Ca is lower in synthetic ACC than in calcite; this reduces the effective radius of its coordination sphere and, hence, the molar volume of the Ca-rich framework relative to the corresponding value in calcite. At the other extreme, we can consider the difference in molar volumes between ACC and a cubic-close-packed array of Ca coordination spheres as a measure of the free volume in ACC. One needs an appropriate estimate for the radius of a Ca coordination sphere, and here, we take one-half the nearest-neighbor Ca···Ca separation of ~4 Å. This comparison gives $\phi = 0.4403$ and $1 - \phi = 0.5597$, which we expect to provide an upper bound to the true free volume. The critical free volume fraction, $\phi_c = 0.2896$, lies between these two estimates and is actually closer to the lower-bound estimate given by the "calcite model". This suggests that the volume fraction of Ca-poor channels in ACC is close to the critical percolation limit and probably safely within the percolating regime. Indeed, in our ACC model, we observe a percolation pathway from one side of the RMC box to the other (Figure 5).

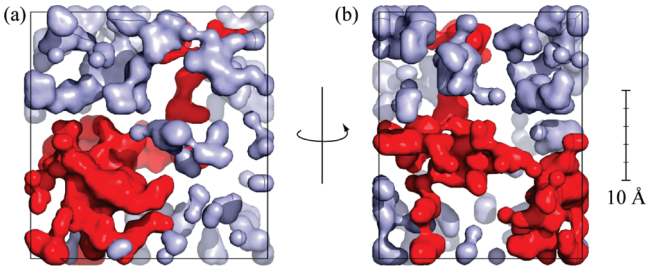

Figure 5. Two views (rotated around vertical axis) showing a percolating Ca-deficient channel (in red) in our RMC model of ACC.

3.2.3. Medium-Range Order. Evidence for Ca clustering comes from the PDF obtained directly from the total scattering data. Beyond the first coordination sphere, the most pronounced interatomic correlations occur at separations of ~4 and ~6 Å (Figure 1b). Our RMC model reflects these oscillations primarily in the Ca···Ca correlations and Ca···O correlations; the correlations between atoms in CO_3 and H_2O units are generally too broad to provide a sufficiently structured contribution to the PDF even at this distance (Figure 6). These two specific Ca···Ca separations have an identifiable structural origin. The ~4 Å peak corresponds to Ca···Ca pairs that are bridged by an oxygen atom in a single carbonate or water group; the ~6 Å peak corresponds to Ca···Ca pairs that are bridged by entire carbonate groups (Figure 6e). Because of the nearest neighbor O coordination around Ca atoms, there are associated peaks in the Ca···O partial at ~4 and ~6 Å, although the 4 Å peak is slightly broader presumably because of the variable Ca coordination (Figure 6). What is key is that these features in the Ca···Ca partial at 4 and 6 Å cannot be reproduced if the Ca atoms are distributed homogeneously throughout the ACC model, even when this distribution is subject to the same geometric constraints used in our RMC refinement. A homogeneous distribution of Ca atoms produces a featureless, hard-sphere-like partial PDF (Figure 6c).

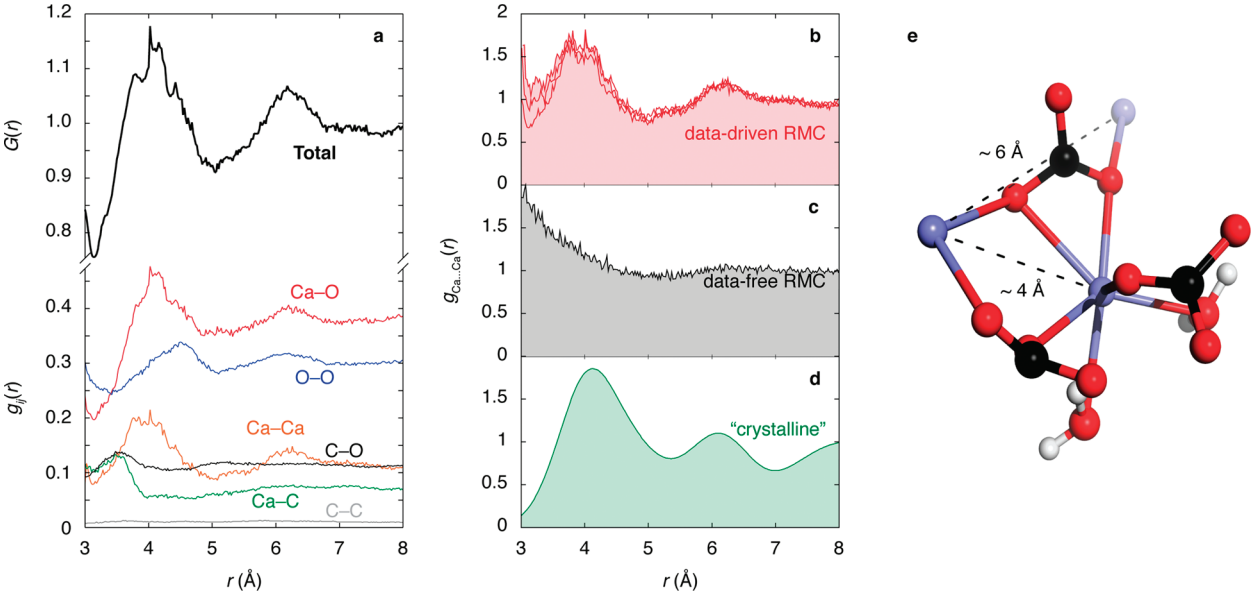

Figure 6. Interpretation of medium-range order in the PDF. (a) RMC total ($G(r)$, bold line) and partial ($g_{ij}(r)$, thin lines) X-ray pair distribution functions calculated from the RMC model using the dMHC-1 initial configuration. The $g_{ij}(r)$ have been scaled by factors of $c_i c_j Z_i Z_j / (\Sigma_i c_i Z_i)^2$ to show their relative contributions to the overall calculated $G(r)$. (b) Ca···Ca partial PDFs from three independent RMC refinements with different starting models provide an indication of their reproducibility among RMC fits. (c) A homogeneous distribution of Ca atoms subject to the same geometric constraints used in the main RMC refinement produces a featureless hard-sphere-like partial PDF, showing that the medium-range order in (a, b) signals a nonhomogeneous distribution of Ca atoms in ACC. (d, e) The two maxima in the Ca···Ca partial PDF are also seen in a broadened "average" PDF calculated from the PDFs of calcite, vaterite, and aragonite; these maxima correspond to Ca pairs connected by a single O atom ($r \sim 4$ Å) and by a whole CO_3^{2-} group ($r \sim 6$ Å).

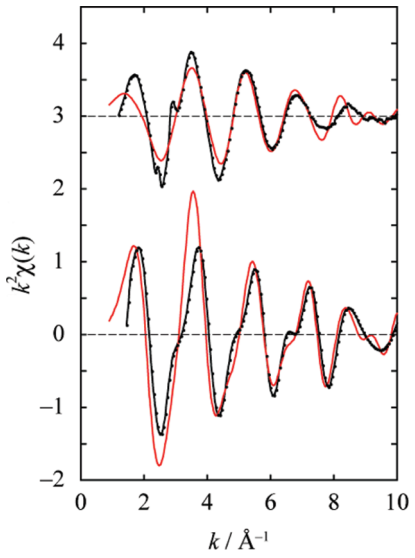

Figure 7. Comparison of experimental (black lines, dots) and calculated (red lines) Ca K-edge EXAFS spectra for amorphous calcium carbonate (top) and calcite (bottom). The small peaks visible in the experimental ACC spectrum at 2.4 and 2.9 Å^{-1} are attributable to multielectron excitations.

These basic Ca···Ca correlations are of course common to the crystalline calcium carbonate forms, and indeed, an average PDF calculated[34] from the crystalline polymorphs into which ACC is known to transform (calcite, vaterite, and aragonite) shows the very same Ca···Ca correlations (Figure 6d). Consequently, the Ca-rich component of ACC effectively assumes the Ca packing density of the crystalline calcium carbonates, with the lower overall density of ACC reflecting the presence of the Ca-poor carbonate/water channel regions. Evidence for preorganization in ACC, specifically a similarity of the local structure around Ca with respect to a crystalline polymorph, has been noted in several EXAFS studies,[11−13] although over shorter length scales and not in the spatial context provided by our model. Furthermore, the entire range of Ca coordination environments exhibited by all the crystalline forms are present in our model. Our model also reflects variability in the linkage between calcium atoms and carbonate groups. On average, 45% of the Ca−CO_3 linkages are bidentate (i.e., edge-sharing). Interestingly, though, the Ca−CO_3 linkage unique to calcite, an exclusively monodentate, corner-sharing arrangement, is not a common motif in our model.

In order to determine if the local structure in our RMC structure model is consistent with Ca K-edge EXAFS results, we calculated the EXAFS function using FEFF7 with the positional coordinates from our model. There is very good correspondence between the experimental data[19] and our calculated spectrum, although not surprisingly the absolute amplitudes differ somewhat (Figure 7). As shown in Figure 7, similar amplitude differences also occur in the comparison of the EXAFS spectrum calculated from the RMC model for calcite with the experimental EXAFS data for calcite. This largely reflects that our FEFF7 calculation did not explicitly account for empirical factors and k-dependent amplitude effects. Nevertheless, the agreement in signal periodicity confirms that our structure model for ACC is consistent with EXAFS results.

3.3. Implications for Stabilization and Transformation of Hydrated ACC. With the packing density of Ca atoms in the ACC similar to that in crystalline forms, the likely pathway for conversion of hydrated ACC into crystalline calcium carbonate would appear to involve a shift of carbonate from the channel regions to the framework and expulsion of water molecules coordinated to Ca from the framework, the latter possibly facilitated by the pore system (Figure 4). The Ca-rich framework and the channels are strongly interlinked so that only small movements would be necessary to coordinate CO_3 units in the pore system with Ca atoms; most CO_3 units are already coordinated with Ca atoms. If this were to proceed stepwise, with water loss occurring first, one might expect that a mostly anhydrous ACC would occur as an intermediate phase, not unlike recent observations in biological ACC that ultimately transforms to calcite.[18] Appearance of intermediate crystalline phases, e.g., vaterite, is also not unlikely, given the wide range of local coordination environments around Ca atoms.

A percolating channel network also suggests possible mechanisms by which additives might stabilize ACC and influence its crystallization pathway. Many of the additives thought to stabilize ACC are anionic, subnanometer-sized molecules, such as triphosphate or phytate anions.[35,36] Similarly, stabilizing proteins are rich in anionic polypeptides that contain a series of glutamate residues;[37] indeed much of the stabilizing activity of such proteins can be simulated by anionic polymers such as polyacrylate or polyaspartate.[38,39] Whereas the channel dimensions that we describe here for an additive-free ACC are clearly smaller than proteins, they appear to be large enough to accommodate smaller subnanometer molecules. This raises the question of whether the pore size and function may be sensitive to the type and properties of different additives. In future work, one could determine how different additives modify the nanopore network. The nanopore structure may, therefore, be the site for direct incorporation of additives within the ACC matrix itself, perhaps facilitated by substitution for carbonate. If additives are located within the pore network, charge neutralization of the framework would be inhibited and the system would be trapped in its charge-separated, amorphous state. One would also expect that carbonate ion orientations within the Ca-rich framework might be influenced by additives within the pore system, and this could allow for some control over polymorph selection during crystallization.

(34) Proffen, T.; Billinge, S. J. L. *J. Appl. Crystallogr.* **1999**, *32*, 572–575.
(35) Clarkson, J. R.; Price, T. J.; Adams, C. J. *J. Chem. Soc. Faraday Trans.* **1992**, *88*, 243–249.
(36) Xu, A.-W.; Yu, Q.; Dong, W.-F.; Antonietti, M.; Colfen, H. *Adv. Mater.* **2005**, *17*, 2217–2221.
(37) Aizenberg, J.; Lambert, G.; Addadi, L.; Weiner, S. *Adv. Mater.* **1996**, *8*, 222–226.
(38) Raz, S.; Weiner, S.; Addadi, L. *Adv. Mater.* **2000**, *12*, 38–42.
(39) Gower, L. B.; Odom, D. J. *J. Cryst. Growth* **2000**, *210*, 719–734.

The most prevalent cationic stabilizer of ACC, namely, Mg^{2+},[7] is known to favor precisely the type of H_2O-rich, low-coordination-number metal environments we find in the framework component of our ACC model, and this may suggest a second mode of stabilization. One might even speculate that movement of Mg^{2+} between the framework and pores could affect charge separation, thereby destabilizing the structure. Finally, the partitioning of chemical dopants, such as PO_4^{3-}, across the rigid framework and pore system of biogenic ACC samples may contribute to the wide variation in stability and structural behavior observed throughout the ACC family.[1]

One of the obvious questions relating to the nanoporous structure is whether the connected channels permit transport of molecules. Given the size of the pores, transport would seem unlikely except possibly for the smallest ions. However, the connected channel network would seem to be the most likely pathway for localized movements of H_2O and CO_3 and may be important during crystallization.

4. Conclusions

We have shown that the atomic-level structure of synthetic, hydrated ACC samples, while lacking long-range order, possesses longer-range structure than indicated by EXAFS alone. It consists of a nanoporous, cationic Ca-rich framework and a carbonate/water component that occupies a connected channel network, resulting in a system that is inherently electrostatically unstable. Our model exhibits a range of Ca coordination environments that encompasses those of the crystalline calcium carbonate polymorphs. Carbonate and water molecules in the channel network are coordinated mainly by hydrogen bonding. We infer that the cationic framework is neutralized by its anion-dominated pore network during crystallization, and the instability of this hydrated ACC with respect to the crystalline polymorphs of calcium carbonate must include the thermodynamic cost of maintaining charge separation on the nanometer scale. We speculate that the existence of a channel network allows ACC to be stabilized by accommodating various additives, which have been shown to stabilize ACC. The general feature of our structural model, namely, a nanoporous charge-separated framework (NCSF), might be expected to recur throughout other examples of ACC, including some biogenic samples, and indeed throughout a number of other biologically relevant materials, including amorphous phosphates and silicates.[40] RMC modeling has successfully been applied to understand inhomogeneous distributions of structural components in fast ion-conducting phosphate and borate glasses.[41,42] Biomimetic approaches to amorphous-precursor materials synthesis are now well-placed to exploit the concept of stabilized NCSFs as a generic synthetic strategy. More generally, we anticipate that the RMC methodology exploited here will allow a number of important outstanding problems in amorphous structural science to be addressed, not simply in terms of biomimetic synthesis or biomineralization but also where relevant structural ambiguities remain in fields where traditional structure approaches have had limited success.

Acknowledgment. A.L.G. gratefully acknowledges Trinity College, Cambridge, and the EPSRC (UK) for the provision of financial support. Support for B.L.P. and R.J.R. was provided by US DOE-BES Grant DE-FG02-09ER16017. Support for F.M.M. was provided by NSF Award CHE-0221934. We thank Dr. Matt Tucker (ISIS) for performing the EXAFS spectra calculations on our RMC models and Drs. Peter J. Chupas and Peter L. Lee of the Advanced Photon Source for assistance in X-ray data collection. We are grateful for access to the Advanced Photon Source, which is supported by the U.S. Department of Energy, Office of Science, Office of Basic Energy Sciences, under Contract No. DE-AC02-06CH11357. Comments from three anonymous reviewers improved the manuscript.

Supporting Information Available: A description of sample synthesis methods, constraints used in RMC refinement (including table of values), and procedure for determination of molar

(40) Simkiss, K. *Bull. de l'Institut océanogr.* **1994**, *14*, 49−54.
(41) Swenson, J.; McGreevy, R. L.; Börgesson, L.; Wicks, J. D. *Solid State Ionics* **1998**, *105*, 55–65.
(42) Swenson, J.; Karlsson, C.; Börgesson, L.; Heenan, R. K. *Phys. Rev. B* **2001**, *64*, 134201.